frontiers | Frontiers in Neuroscience

TYPE Perspective
PUBLISHED 18 May 2023
DOI 10.3389/fnins.2023.1135494

OPEN ACCESS

EDITED BY
Panagiotis Symvoulidis,
Massachusetts Institute of Technology,
United States

REVIEWED BY
Riccardo Marin,
University of Ottawa, Canada

*CORRESPONDENCE
Bernardo A. Arús
✉ bernardo.arus@nct-dresden.de
Oliver T. Bruns
✉ oliver.bruns@nct-dresden.de

RECEIVED 31 December 2022
ACCEPTED 24 April 2023
PUBLISHED 18 May 2023

CITATION
Arús BA, Cosco ED, Yiu J, Balba I, Bischof TS, Sletten EM and Bruns OT (2023) Shortwave infrared fluorescence imaging of peripheral organs in awake and freely moving mice. *Front. Neurosci.* 17:1135494. doi: 10.3389/fnins.2023.1135494

Shortwave infrared fluorescence imaging of peripheral organs in awake and freely moving mice

Bernardo A. Arús[1,2,3,4,5]*, Emily D. Cosco[1,6], Joycelyn Yiu[1], Ilaria Balba[1], Thomas S. Bischof[1,2,3,4,5], Ellen M. Sletten[6] and Oliver T. Bruns[1,2,3,4,5]*

[1]Helmholtz Pioneer Campus, Helmholtz Zentrum München, Neuherberg, Germany, [2]German Cancer Research Center (DKFZ), Heidelberg, Germany, [3]National Center for Tumor Diseases (NCT/UCC), Dresden, Germany, [4]Medizinische Fakultät and University Hospital Carl Gustav Carus, Technische Universität Dresden, Dresden, Germany, [5]Helmholtz-Zentrum Dresden-Rossendorf (HZDR), Dresden, Germany, [6]Department of Chemistry and Biochemistry, University of California, Los Angeles, Los Angeles, CA, United States

Extracting biological information from awake and unrestrained mice is imperative to *in vivo* basic and pre-clinical research. Accordingly, imaging methods which preclude invasiveness, anesthesia, and/or physical restraint enable more physiologically relevant biological data extraction by eliminating these extrinsic confounders. In this article, we discuss the recent development of shortwave infrared (SWIR) fluorescent imaging to visualize peripheral organs in freely-behaving mice, as well as propose potential applications of this imaging modality in the neurosciences.

KEYWORDS

optical imaging, fluorescence, *in vivo* imaging, awake imaging, fluorescent dyes, near infrared (NIR)-II, organic fluorophores, polymethine dyes

Introduction

The study of physiology in living animals is often limited by the requirement of invasive procedures, physical restraint, anesthesia, or even euthanasia. Tissue biopsies and blood-based assays require animal manipulation and restraint, increasing stress levels, which inevitably affects general animal physiology (Kvetnansky et al., 1978; Pare and Glavin, 1986; Glavin et al., 1994; Buchecker et al., 2020). Likewise, anesthesia impacts a plethora of physiological parameters, including brain function and energy metabolism (Dobkin et al., 1966; Grandjean et al., 2014; Lundgaard et al., 2015; Sano et al., 2016; Bachmann et al., 2019; Bascunana et al., 2019). In addition, correlative or causal studies of the relationship between tissue function and behavior are not possible when animals are in an anesthetized state. Therefore, enabling non-invasive measurements without confounders induced by physical and chemical restraint provides striking progress on pre-clinical research (Lundgaard et al., 2015; Sano et al., 2016; Buchecker et al., 2020).

Most non-invasive, contact-free imaging methods, such as computed tomography (CT) and magnetic resonance imaging (MRI), have limited application in freely-moving mice due to their low temporal resolution, field-of-view requirements, and limited sensitivity for contrast agents (James and Gambhir, 2012; Phinikaridou et al., 2012; Lauber et al., 2017). Positron emission tomography (PET) measurements have overcome some of these limitations and recently enabled unrestrained awake mouse imaging (Miranda et al., 2019a,b). Optical techniques arise as an alternative given their high acquisition rate and potential to be coupled with fluorescent agents

to provide structural, functional, genetic, or metabolic contrast in freely behaving mice (Villette et al., 2019; Wang et al., 2021; Yang et al., 2021). One major caveat of using light in biological specimens is the limited light penetration through tissue; however, near-infrared (NIR, 700–1,000 nm) and shortwave infrared (SWIR, 1,000–1,700 nm) fluorescence imaging have excelled to provide high resolution visualization of biological structures through the mouse skin, including the brain vasculature (Cosco et al., 2017, 2020, 2021; Carr et al., 2018b; Zhong et al., 2019; Wang et al., 2021).

The SWIR region of the electromagnetic spectrum presents photophysical properties that make it the optimal regimen for optical *in vivo* imaging, given its optical properties, including (a) high tissue translucence; (b) deeper light penetration in tissue at longer wavelengths; (c) negligible tissue autofluorescence; and (d) higher absorbance of light by water molecules, thereby increasing superficial contrast (Carr et al., 2018a,b; Ding et al., 2018). Exploring these favorable properties, a number of SWIR-emissive probes, including the clinically-approved agent indocyanine green (ICG) and related organic dyes, as well as quantum dots, carbon nanotubes, and rare-earth doped nanoparticles have been recently developed or applied to enable biomedical applications of SWIR imaging (Hong et al., 2014a; Hong and Dai, 2016; Bruns et al., 2017; Cosco et al., 2017, 2020, 2021; Carr et al., 2018b; Ortgies et al., 2018; Zhong et al., 2019; Xu et al., 2020; Ximendes et al., 2021; Bandi et al., 2022). Furthermore, advances in the technology of SWIR-sensitive cameras, such as InGaAs-based detectors, have also enabled increased resolution, sensitivity and efficiency. In essence, the development of bright contrast agents, high-speed and sensitive InGaAs cameras, combined with compatible optics, have enabled researchers to push the limits of deep tissue imaging with unprecedented speed and resolution (Zhong et al., 2019; Cosco et al., 2021).

In vivo SWIR imaging has been applied to detect vascular networks, assess metabolic activity, visualize lymphatic vessels, and monitor vital signs in mouse models (Bartelt et al., 2011, 2018; Bruns et al., 2017; Cosco et al., 2020; Bandi et al., 2022). While most of these applications have been demonstrated in anesthetized animals, a few reports have shown the ability to employ SWIR imaging to freely-moving mice (Bruns et al., 2017; Li et al., 2018; Cosco et al., 2020). Here we present data on the application of SWIR fluorescence imaging to visualize biological parameters in fully awake and freely moving mice. Combining high contrast SWIR-emitting fluorophores with SWIR-detecting technology, we enabled real-time, multi-channel video recording of up to 4 different channels with subsequent tracking of organs of interest, including liver, brown adipose tissue (BAT), intestines, vasculature and peritoneal space, from freely roaming and behaving mice. In context of these new results, we discuss the challenges and perspectives of deploying this modality to complement brain imaging or to directly image brain activity.

Experimental strategy for optical imaging in freely behaving mice

In this study, we employ recently-established bright SWIR-emissive organic dyes which enabled acquisition with exposure times in the range of 1–10 ms for non-invasive awake mouse imaging. For optimal dye excitation, we chose those with absorption spectra matched to commercially available NIR and SWIR laser lines. We thus selected the contrast agents ICG, JuloChrom5, Chrom7, and JuloFlav7 to, respectively, match lasers with peak at 785, 892, 962, and 1,064 nm (Cosco et al., 2020, 2021) (Supplementary Figure S1). Apart from ICG, which is water soluble, the dyes were encapsulated in lipid micelles for injection *in vivo*. To detect SWIR fluorescence emission of organs from awake mice, we used a 35-mm F/1.4 lens providing mouse whole-body field of view and a monochrome InGaAs detector with maximal frame rate of 300 frames per second (fps) at 640 × 512 pixels resolution. The detection window was selected by 1,000- or 1,150-nm long-pass filters, depending on the fluorophores and laser lines used in each experiment.

Fast acquisition is required for imaging freely behaving mice

Imaging awake and freely moving mice requires high temporal and spatial resolution as well as favorable contrast settings to resolve biological parameters of interest while accounting for the animal motion. For example, in a natural movement such as a mouse shaking and itching its head, we show that an exposure time in the order of 10 ms (equivalent to 100 fps) is necessary to resolve major fluorescently-labeled blood vessels. However, some smaller vessels can only be observed at 3 ms (in this case acquired at 300 fps) (Figure 1A). Novel SWIR-emitting fluorophores with enough brightness to achieve this exposure time at safe laser power densities (International Commission on Non-Ionizing Radiation P, 2013) have been recently developed (Zhong et al., 2019; Santos et al., 2020; Cosco et al., 2021), and the current SWIR detection technology surpasses the required frame rates, therefore paving the way for SWIR fluorescence imaging in freely-behaving mice.

Labeling and visualizing major blood vessels in awake and freely moving mice

To enable vasculature labeling, a long-circulating micelle formulation of Chrom7 was intravenously (i.v.) injected, allowing for imaging sessions for at least 1 h post-injection. Imaging at 45 min after injection, we observed signal concentrated in major vessels around the orbits, the base of the skull and hind limbs (dorsal view, Figure 1B and Supplementary Video S1). These images were acquired at 300 fps, using a 968-nm illumination source and 1,000 nm long-pass filtering. To showcase the resolution maintained when acquiring at this frame rate, we slowed down the video display speed from 300 to 30 fps; the fast mouse movement was then showed in slow motion, and most of the vessels could still be resolved (Supplementary Video S2). This highlights that fluorescence SWIR imaging can be used to resolve fine structures in a mouse exhibiting its natural behavior, while maintaining a large, whole-mouse field of view.

Fluorophore multiplexing enables orthogonal imaging of biological tissues in socially interacting mice in up to 4 channels

One way to exploit the speed enabled by SWIR-emitting fluorophores is by acquiring images in multiple channels, a pivotal feature in pre-clinical imaging studies (Li et al., 2020; Tian et al., 2020;

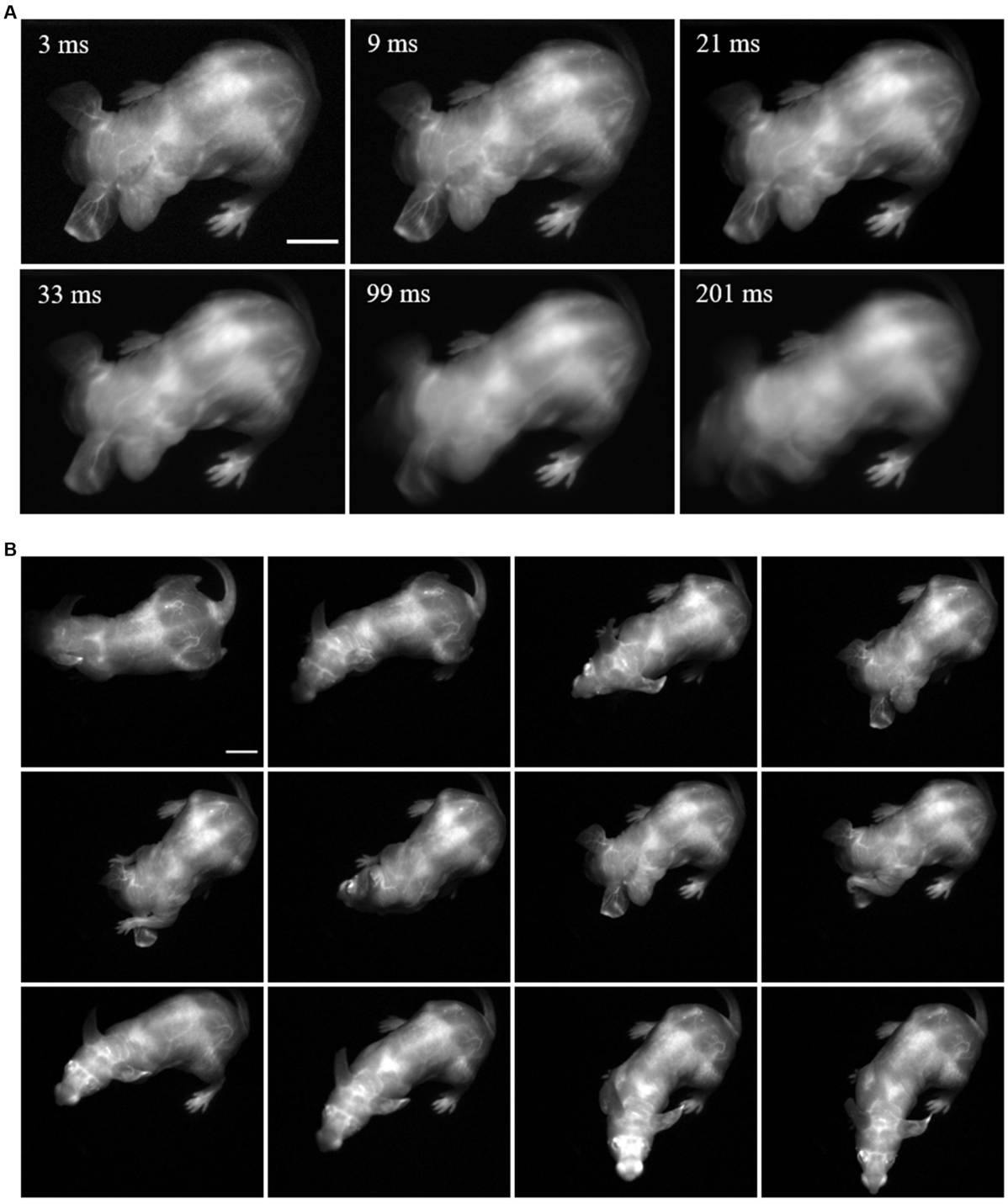

FIGURE 1
Fast acquisition speed is required for imaging of fine mouse vasculature in awake and freely moving mice. A freely behaving mouse with its vasculature labeled with Chrom7 micelles was dorsally imaged with an InGaAs detector (3 ms exposure time; 1100-nm long-pass filter; excitation at 968 nm (100 mW/cm^2). **(A)** Comparison between a single frame acquired at 3 ms, and the average of this frame with its adjacent ones, comprising simulated exposure times of 9, 21, 33, 99, and 201 ms. **(B)** Selected frames of SWIR fluorescence vascular imaging in the mouse freely moving in the imaging chamber. Minimum and maximum displayed values are 0 and 65, respectively. Scale bar: 1 cm.

Bandi et al., 2022). For multiplexed imaging, we made use of the excitation-multiplexing concept: fluorophore excitation-matched laser wavelengths were turned on in alternating sequence while fluorescence emission was collected in a single detection window using a single set of long-pass filters (Figure 2A and Supplementary Figure S1). This multiplexing strategy (thoroughly discussed by Cosco et al. (2020)) not only favors speed, given the absence of moving parts to change emission filters, but also maintains consistent resolution and contrast, which are strongly dependent on detection wavelength in the NIR and SWIR windows.

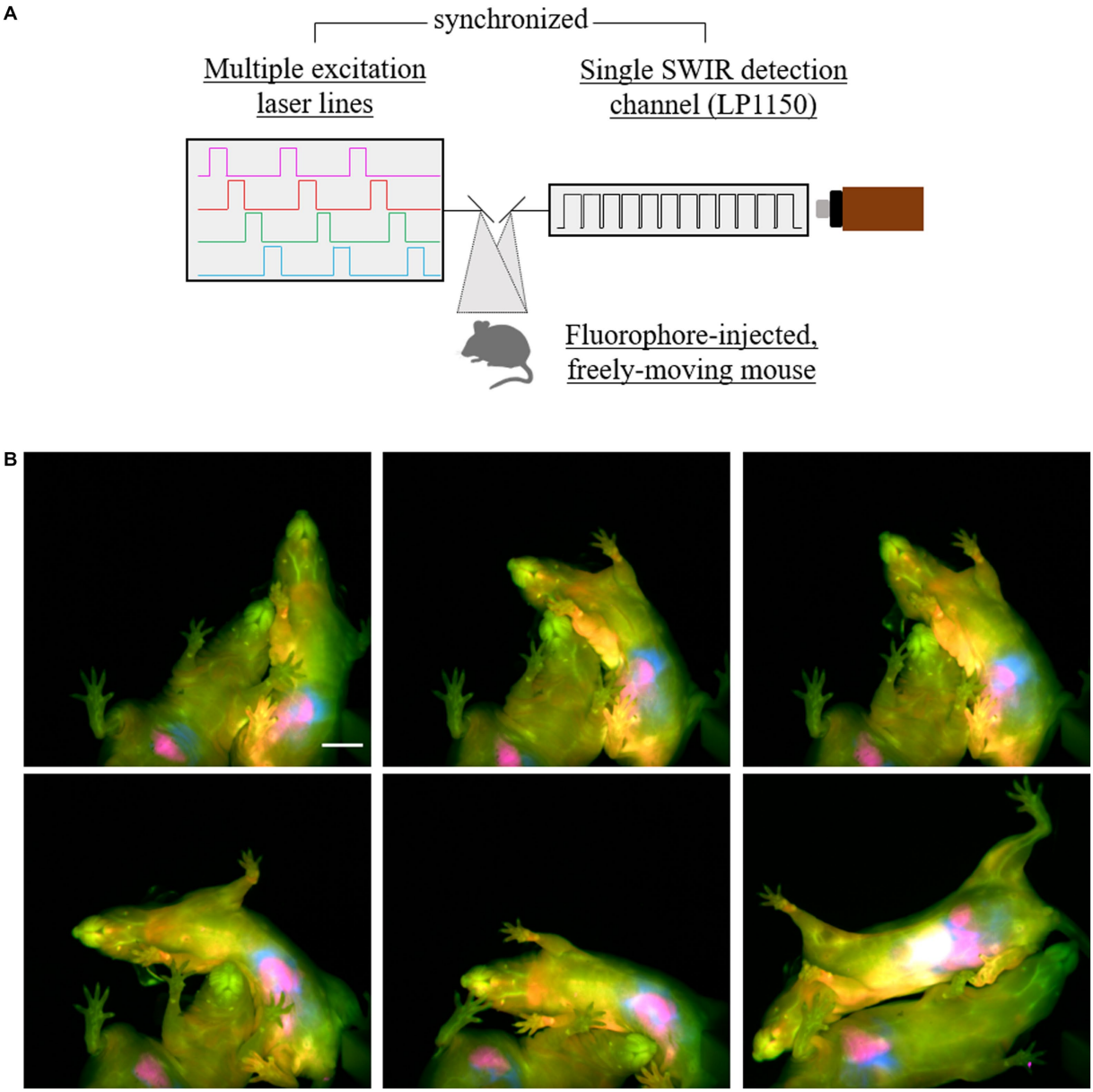

FIGURE 2
Four-color SWIR fluorescence imaging of socially interacting mice. **(A)** Diagram of the multiple-fluorophore imaging strategy, showing four different lasers matching the excitation spectra of four selected fluorophores were synchronized with an InGaAs detector using an 1150 nm long-pass filter (7.8 ms exposure time per frame; 32 frames per second effective framerate in the four-channel, merge images). **(B)** Two mice had ICG labeling in the intestines (magenta, 6 h after intravenous (i.v.) injection), JuloChrom5 in macrophage-rich organs, such as liver, bones, and lymph nodes (red, 24 h after i.v. injection), Chrom7 in the blood vasculature (green, 15-30 min after i.v. injection), and JuloFlav7 in the intraperitoneal space (30-45 min after i.p. injection). Lasers 785 nm (49 mW/cm^2), 892 nm (81 mW/cm^2), 968 nm (113 mW/cm^2), and 1064 nm (165 mW/cm^2) were used to excite ICG, JuloChrom5, Chrom7, and JuloFlav7, respectively. These mice were imaged ventrally while exploring the imaging chamber and socially interacting. Minimum and maximum displayed values are: a) ICG: 1000 and 1900; b) JuloChrom5: 400 and 850; c) Chrom7: 300 and 1750; d) 100 and 1750. Scale bar: 1 cm.

To label different biological structures of interest, we deployed different injection strategies and exploited the distinct biodistribution of the fluorophores' formulations. Circulating ICG molecules are rapidly taken up by hepatocytes in the liver, from which it is excreted through the biliary tract to the intestinal tract (Meijer et al., 1988; Bahmani et al., 2013). Depending on the time after injection, the liver and/or the intestines can be visualized with a high signal-to-background ratio (Bahmani et al., 2013; Cosco et al., 2021). To visualize the intestines, mice were imaged 5–6 h after an intravenous (i.v.) ICG injection. Macrophage-rich organs, such as liver, lymph nodes, and bones, are rich in signal 24 h after JuloChrom5 micelles intravenous (i.v.) injection (Cosco et al., 2021); we used this strategy to provide bone/anatomical contrast. JuloFlav7 micelles were injected intraperitoneally 30–90 min before imaging, to provide complementary information in the peritoneal cavity, alongside the ICG-labeled intestines. Finally, to label the vasculature, the

long-circulating Chrom7 micelles were injected intravenously (i.v.) 15–30 min before imaging. Using the same experimental approach, we imaged two cage mates socially interacting in the imaging arena (Figure 2B; Supplementary Figure S2; Supplementary Videos S3, S4), which is naturally not possible if mice are anesthetized. For this experiment, we used an 1,150 nm long pass filter which reduced the total collected light, hence we increased the exposure time to 7.8 ms. The effective frame rate of the final 4-channel video is 30 fps, therefore maintaining video rate speed, but decreasing our ability to resolve small structures when the mouse exhibits particularly quick movements.

The excitation spectra of these dyes present some overlap/crosstalk among the excitation channels. In previous three- and four-color multiplexed reports on anesthetized mice we used linear unmixing to separate each channel and circumvent these issues. However, linear unmixing relies on the assumption that the emission response of fluorophores is linear across different excitations [discussed in detail by Cosco et al. (2021)]. Fluorophore response, however, turns out to mildly deviate from linearity in geometrically different organs (e.g., vessels vs. liver vs. deep lymph nodes). While not affecting the visual separation of the channels in the published multi-color image of anesthetized mice, this effect does make the images no longer quantitative. Notably, organ geometry considerably changes according the various poses presented by the mice while roaming around. Therefore, to minimize fluorophore crosstalk and avoid the need of post-processing tools to differentiate the channels, we progressively decreased contrast agent concentration while increasing the incident laser power density in a wavelength-dependent manner. This resulted in distinguishable imaging channels (Figure 2B), without the need of unmixing algorithms, despite the presence of some fluorophore crosstalk in the individual channels (Supplementary Figure S2). Improving raw data acquisition processes provides a next step to enable future quantitative multiplexed imaging of awake mice.

Organ tracking from freely behaving mice

In order to extract physiologically relevant data from a video with labeled organs, the location of each organ needs to be determined. A number of approaches to tackle this challenge in anesthetized mice have been developed, for instance using manual annotation/selection of regions of interest (ROIs), PCA analysis, or image segmentation (Wang et al., 2006; Hillman and Moore, 2007; Schoppe et al., 2020). PCA analysis relies on the temporal signature of the contrast agent, which requires the organs to be immobile, hence being not applicable to datasets with awake and freely moving mice (Hillman and Moore, 2007). Manual ROI selection proves cumbersome to perform in large datasets, for example when acquiring at 300 fps.

We initially tried to solve this by thresholding the whole awake mouse dataset according to a pre-set intensity value. However, we found this approach inconsistent due to the reliance on intensity values, difference in mouse pose/posture, remains of contrast agent in the tail, and poor performance in low signal-to-background samples. Reckoning that delineation of organs contour by segmentation would also face similar challenges, we opted to track mouse organs using mouse tracking algorithms which are typically used for pose estimation.

Mouse tracking and pose estimation are widely investigated problems in computer vision with particular application in neuroscience and ethological studies (Dell et al., 2014; Gris et al., 2017; Abbas and Masip, 2019; Datta et al., 2019). These techniques are used to predict and track an animal position and orientation, usually providing behavioral and motion information after the application of different stimuli. Here, we adopted DeepLabCut (Mathis et al., 2018), a deep learning approach, to predict the position of an organ in freely moving mice. Particularly, models were trained which were capable of tracking, for example the paws, BAT, liver, intestines and heart regions.

DeepLabCut is a deep convolutional neural network used for mouse tracking and pose estimation (Mathis et al., 2018). It relies on a user-defined pre-selection of coordinates delineating a structure of interest (usually the whole mouse) to predict its shape and location in the remaining video frames. To apply the algorithm to organ tracking, we first defined manual ROI selection (markers) around the organ of interest on a fraction of the dataset (typically 10% of the frames per experiment). These markers were placed not only on the target structure, but also on peripheral structures to enable the alignment of the entire mouse (dorsal side or ventral side). This initial selection was then used by DeepLabCut to train its own convolutional neural network, and finally use the trained model to predict the location of each region on the remaining frames, providing as output an XY-coordinate list of the predicted ROI location for each frame (Supplementary Figure S3). The likelihood values associated with the markers were used to filter out incorrectly labeled frames.

To help future data extraction, we added a few steps to the processing pipeline, with the aim to output a stack of frames of transformed (translated and rotated) mice facing up. To achieve that, each marker for the target structure was translated to the center of the field of view, and peripheral markers were rotated about the central marker so that the posture of the mouse was aligned across different frames (Supplementary Figure S3). Finally, ROIs can be drawn over the target structure of the resulting aligned image stack to eventually be used to extract quantitative information from the tracked organs. Using this processing pipeline, one could generate tracking videos of, e.g., the BAT, liver or paw blood vasculature regions of awake mice roaming around the imaging chamber, ten-fold faster than with manual annotation, with room for scalability and efficiency improvement.

Challenges and perspective to the use of SWIR fluorescence imaging in neuroscience research

The pipeline for macroscopic SWIR fluorescence imaging presented here might seem far off from neuroscience applications, which typically rely on data from single cells, neuronal populations, or at the very least brain regions. The macroscopic resolution shown above clearly does not compare to that obtained by surgically-implanted sensors, such as patch-clamp, photometry, or optogenetic probes, which enable awake imaging, but possess an invasive character, despite recent advances to bypass invasive surgical procedures (Cui et al., 2014; Chen et al., 2021; Noguchi et al., 2021; Linders et al., 2022). The same is true for the resolution of other optical methods, such as two-photon microscopy and miniaturized microscopes, which require cranial window implantation and mouse restraining (Dombeck and

Tank, 2014; Ozbay et al., 2018), and fMRI, which has low temporal resolution and also rely on restraining (Desjardins et al., 2019). Of note, mesoscopic SWIR imaging has been used to visualize small brain vessels or blood–brain-barrier leakage through skin and skull in anesthetized mice (Hong et al., 2014b; Zhang et al., 2016; Carr et al., 2018b). Nevertheless, non-invasive imaging of brain dynamics or parameters which complement brain imaging in freely behaving mice indicates a plausible perspective for a number of potential applications.

Calcium imaging, widely used by neuroscientists to visualize neuronal dynamics, is one immediate such candidate (Yang and Yuste, 2017). Genetically-encoded calcium indicators, such as those based on GCaMP and more recent red-shifted probes, are used as surrogate for activity of specific neuronal subtypes (Qian et al., 2019; Shemetov et al., 2021; Kim and Schnitzer, 2022). While a remarkable application of this technique is based on three-dimensional and/or single-cellular imaging, it is also used at a larger scale in wide-field imaging to detect coordinated activity in specific brain regions, particularly in the cerebral cortex (Ren and Komiyama, 2021). The latter has also been applied to restrained awake mice with an implanted cranial window (Barson et al., 2020). We here report the ability of SWIR fluorescence imaging to clearly visualize the cerebral sinuses in awake and freely-moving mice, and to image multiple channels in these mice. Using a similar acquisition setup and processing pipeline to correct for motion, it is conceivable to track slow-moving signals like the neuronal activity waves seen with GCaMP, while the mouse exhibits certain behaviors, especially natural ones prevented by head-fixing. A related potential approach is the measurement of brain hemodynamics under different conditions and stimuli, or the combination of such studies with neuronal activity modulators, such as chemogenetic tools, which use conserved signaling pathways and also have a non-invasive nature (Zhang et al., 2016; Bruns et al., 2017; Atasoy and Sternson, 2018). Moreover, blood–brain-barrier leakage studies could also be pursued in freely-moving animals. Performing such studies in awake animals, besides enabling correlative measurements between behavior and physiology, eliminates confounders introduced by anesthesia and stress by restraining (Aksenov et al., 2015; Sano et al., 2016).

The ability of non-invasive macroscopic SWIR imaging to visualize other organs, such as the intestines and liver, also indicates that chemogenetic studies could be designed to investigate the causal factor of neuronal excitation/inhibition in the physiology of peripheral organs, therefore enabling the non-invasive direct visualization of brain-organ crosstalk studies in freely behaving mice. For instance, ICG is a SWIR-emissive fluorophore clinically used to evaluate liver physiology (Schwarz et al., 2019); thus, combining these techniques, brain-liver crosstalk studies could be pursued without the interference of restraining and anesthesia. Also in the context of brain-organ crosstalk, fluorescent agents targeting pathogenic or commensal bacterial species could be applied in gut microbiota-brain axis studies, similarly to PET tracers (Giron and Mazzi, 2021). SWIR fluorescence has also been used to label glioma cells (Bruns et al., 2017; Li et al., 2022). We envision that labeled glioma could be monitored in parallel with behavioral measurement and/or in combination with hemodynamic or chemogenetic measurements.

Recent efforts have enabled the leap in mouse brain PET imaging studies from restrained and head-fixed to freely-moving animals (Takuwa et al., 2016; Miranda et al., 2019a). Combining the non-invasive properties of PET and SWIR imaging would allow the measurement of correlated signals in freely behaving mice. One example is the simultaneous assessment of blood flow changes with SWIR fluorescence and fluorodeoxyglucose uptake with PET, while the mice exhibit certain behaviors. Despite deviating from the non-invasive character enabled by SWIR imaging, we finally mention the orthogonality of this modality with other traditional neuronal activity recording and manipulating methods, such as fiber photometry, electrophysiology and optogenetics. The applications here mentioned could be combined with these classical tools to, for instance, combine a peripheral physiological measurement with the real-time on/off optogenetic remote control of specific neuronal populations.

Conclusion

The application of SWIR imaging enables the removal of anesthesia, restraints, implants, and other non-invasive steps to study the animal in a state of being and environment which is as close to natural as possible. In addition, due to its noninvasive nature, SWIR imaging potentially enables the longitudinal investigation of physiological changes in each animal under study, instead of requiring the sacrifice of large populations at each time point. As a result, it would be possible to resolve the individual reaction of each animal to intervention, revealing key features lost in population averaging.

Here we presented the combination of high-contrast SWIR-emitting contrast agents with SWIR-detecting technology to enable real-time, multi-channel video recording of up to 4 different channels with subsequent tracking of organs of interest from freely roaming and behaving mice. Although yet to be demonstrated, the techniques here shown have the strong potential to enable non-invasive brain activity and brain-peripheral organ crosstalk imaging in freely moving mice, therefore unburdening neuroscientists from invasive procedures, anesthesia, or mouse restraining.

Data availability statement

Image data sets, including all raw and processed data generated in this work, are available at BioImage Archive, accession number: S-BIAD680. These data can be obtained without costs via https://www.ebi.ac.uk/biostudies/bioimages/studies/S-BIAD680. The data processing steps used in this manuscript can be found at GitLab, via https://gitlab.com/brunslab/manuscript-awake-mouse-imaging.

Ethics statement

Animal experiments were performed in conformity with institutional guidelines and protocols.

Author contributions

BA, EC, ES, TB, and OB contributed to conception and design of the study. BA and EC executed imaging experiments. JY, IB, and TB worked on the neural network training and implementation. BA and OB wrote the first draft of the manuscript. All authors wrote sections of the manuscript. All authors contributed to the article and approved the submitted version.

Funding

This work was financially supported by the NSF (DGE-1144087 to EC), the NIH (1R01EB027172 to ES), the Foote Family (EC), the Alfred P. Sloan Foundation (FG-2018-10855 to ES), the Emmy-Noether-Program of DFG (BR 5355/2-1 to OB), the CZI Deep Tissue Imaging (DTI-0000000248 to OB), UCLA, and the Helmholtz Pioneer Campus.

Conflict of interest

The authors declare that the research was conducted in the absence of any commercial or financial relationships that could be construed as a potential conflict of interest.

Publisher's note

Supplementary material

The Supplementary material for this article can be found online at: https://www.frontiersin.org/articles/10.3389/fnins.2023.1135494/full#supplementary-material

References

Abbas, W., and Masip Rodo, D. (2019). Computer methods for automatic locomotion and gesture tracking in mice and small animals for neuroscience applications: a survey. *Sensors (Basel, Switzerland)* 19:3274. doi: 10.3390/s19153274

Aksenov, D. P., Li, L., Miller, M. J., Iordanescu, G., and Wyrwicz, A. M. (2015). Effects of anesthesia on BOLD signal and neuronal activity in the somatosensory cortex. *J. Cereb. Blood Flow Metab.* 35, 1819–1826. doi: 10.1038/jcbfm.2015.130

Atasoy, D., and Sternson, S. M. (2018). Chemogenetic tools for causal cellular and neuronal biology. *Physiol. Rev.* 98, 391–418. doi: 10.1152/physrev.00009.2017

Bachmann, S. B., Proulx, S. T., He, Y., Ries, M., and Detmar, M. (2019). Differential effects of anaesthesia on the contractility of lymphatic vessels in vivo. *J. Physiol.* 597, 2841–2852. doi: 10.1113/JP277254

Bahmani, B., Lytle, C. Y., Walker, A. M., Gupta, S., Vullev, V. I., and Anvari, B. (2013). Effects of nanoencapsulation and PEGylation on biodistribution of indocyanine green in healthy mice: quantitative fluorescence imaging and analysis of organs. *Int. J. Nanomedicine* 8, 1609–1620. doi: 10.2147/IJN.S42511

Bandi, V. G., Luciano, M. P., Saccomano, M., Patel, N. L., Bischof, T. S., Lingg, J. G. P., et al. (2022). Targeted multicolor in vivo imaging over 1,000 nm enabled by nonamethine cyanines. *Nat. Methods* 19, 353–358. doi: 10.1038/s41592-022-01394-6

Barson, D., Hamodi, A. S., Shen, X., Lur, G., Constable, R. T., Cardin, J. A., et al. (2020). Simultaneous mesoscopic and two-photon imaging of neuronal activity in cortical circuits. *Nat. Methods* 17, 107–113. doi: 10.1038/s41592-019-0625-2

Bartelt, A., Bruns, O. T., Reimer, R., Hohenberg, H., Ittrich, H., Peldschus, K., et al. (2011). Brown adipose tissue activity controls triglyceride clearance. *Nat. Med.* 17, 200–205. doi: 10.1038/nm.2297

Bartelt, A., Widenmaier, S. B., Schlein, C., Johann, K., Goncalves, R. L. S., Eguchi, K., et al. (2018). Brown adipose tissue thermogenic adaptation requires Nrf1-mediated proteasomal activity. *Nat. Med.* 24, 292–303. doi: 10.1038/nm.4481

Bascunana, P., Thackeray, J. T., Bankstahl, M., Bengel, F. M., and Bankstahl, J. P. (2019). Anesthesia and preconditioning induced changes in mouse brain [(18)F] FDG uptake and kinetics. *Mol. Imaging Biol.* 21, 1089–1096. doi: 10.1007/s11307-019-01314-9

Bruns, O. T., Bischof, T. S., Harris, D. K., Franke, D., Shi, Y., Riedemann, L., et al. (2017). Next-generation in vivo optical imaging with short-wave infrared quantum dots. *Nat. Biomed. Eng.* 1:1. doi: 10.1038/s41551-017-0056

Buchecker, V., Waldron, A. M., van Dijk, R. M., Koska, I., Brendel, M., von Ungern-Sternberg, B., et al. (2020). [(18)F]MPPF and [(18)F]FDG muPET imaging in rats: impact of transport and restraint stress. *EJNMMI Res.* 10:112. doi: 10.1186/s13550-020-00693-3

Carr, J. A., Aellen, M., Franke, D., So, P. T. C., Bruns, O. T., and Bawendi, M. G. (2018a). Absorption by water increases fluorescence image contrast of biological tissue in the shortwave infrared. *Proc. Natl. Acad. Sci. U. S. A.* 115, 9080–9085. doi: 10.1073/pnas.1803210115

Carr, J. A., Franke, D., Caram, J. R., Perkinson, C. F., Saif, M., Askoxylakis, V., et al. (2018b). Shortwave infrared fluorescence imaging with the clinically approved near-infrared dye indocyanine green. *Proc. Natl. Acad. Sci. U. S. A.* 115, 4465–4470. doi: 10.1073/pnas.1718917115

Chen, R., Gore, F., Nguyen, Q. A., Ramakrishnan, C., Patel, S., Kim, S. H., et al. (2021). Deep brain optogenetics without intracranial surgery. *Nat. Biotechnol.* 39, 161–164. doi: 10.1038/s41587-020-0679-9

Cosco, E. D., Arus, B. A., Spearman, A. L., Atallah, T. L., Lim, I., Leland, O. S., et al. (2021). Bright chromenylium polymethine dyes enable fast, four-color in vivo imaging with shortwave infrared detection. *J. Am. Chem. Soc.* 143, 6836–6846. doi: 10.1021/jacs.0c11599

Cosco, E. D., Caram, J. R., Bruns, O. T., Franke, D., Day, R. A., Farr, E. P., et al. (2017). Flavylium polymethine fluorophores for near- and shortwave infrared imaging. *Angew. Chem. Int. Ed. Engl.* 56, 13126–13129. doi: 10.1002/anie.201706974

Cosco, E. D., Spearman, A. L., Ramakrishnan, S., Lingg, J. G. P., Saccomano, M., Pengshung, M., et al. (2020). Shortwave infrared polymethine fluorophores matched to excitation lasers enable non-invasive, multicolour in vivo imaging in real time. *Nat. Chem.* 12, 1123–1130. doi: 10.1038/s41557-020-00554-5

Cui, G., Jun, S. B., Jin, X., Luo, G., Pham, M. D., Lovinger, D. M., et al. (2014). Deep brain optical measurements of cell type-specific neural activity in behaving mice. *Nat. Protoc.* 9, 1213–1228. doi: 10.1038/nprot.2014.080

Datta, S. R., Anderson, D. J., Branson, K., Perona, P., and Leifer, A. (2019). Computational neuroethology: a call to action. *Neuron* 104, 11–24. doi: 10.1016/j.neuron.2019.09.038

Dell, A. I., Bender, J. A., Branson, K., Couzin, I. D., de Polavieja, G. G., Noldus, L. P., et al. (2014). Automated image-based tracking and its application in ecology. *Trends Ecol. Evol.* 29, 417–428. doi: 10.1016/j.tree.2014.05.004

Desjardins, M., Kilic, K., Thunemann, M., Mateo, C., Holland, D., Ferri, C. G. L., et al. (2019). Awake mouse imaging: from two-photon microscopy to blood oxygen level-dependent functional magnetic resonance imaging. *Biol. Psychiatry Cogn. Neurosci. Neuroimaging.* 4, 533–542. doi: 10.1016/j.bpsc.2018.12.002

Ding, F., Zhan, Y., Lu, X., and Sun, Y. (2018). Recent advances in near-infrared II fluorophores for multifunctional biomedical imaging. *Chem. Sci.* 9, 4370–4380. doi: 10.1039/C8SC01153B

Dobkin, A. B., Byles, P. H., and Neville, J. F. Jr. (1966). Neuroendocrine and metabolic effects of general anaesthesia and graded haemorrhage. *Can. Anaesth. Soc. J.* 13, 453–475. doi: 10.1007/BF03003613

Dombeck, D., and Tank, D. (2014). Two-photon imaging of neural activity in awake mobile mice. *Cold Spring Harb. Protoc.* 2014, 726–736. doi: 10.1101/pdb.top081810

Giron, M. C., and Mazzi, U. (2021). Molecular imaging of microbiota-gut-brain axis: searching for the right targeted probe for the right target and disease. *Nucl. Med. Biol.* 92, 72–77. doi: 10.1016/j.nucmedbio.2020.11.002

Glavin, G. B., Pare, W. P., Sandbak, T., Bakke, H. K., and Murison, R. (1994). Restraint stress in biomedical research: an update. *Neurosci. Biobehav. Rev.* 18, 223–249. doi: 10.1016/0149-7634(94)90027-2

Grandjean, J., Schroeter, A., Batata, I., and Rudin, M. (2014). Optimization of anesthesia protocol for resting-state fMRI in mice based on differential effects of anesthetics on functional connectivity patterns. *NeuroImage* 102, 838–847. doi: 10.1016/j.neuroimage.2014.08.043

Gris, K. V., Coutu, J. P., and Gris, D. (2017). Supervised and unsupervised learning Technology in the Study of rodent behavior. *Front. Behav. Neurosci.* 11:141. doi: 10.3389/fnbeh.2017.00141

Hillman, E. M., and Moore, A. (2007). All-optical anatomical co-registration for molecular imaging of small animals using dynamic contrast. *Nat. Photonics* 1, 526–530. doi: 10.1038/nphoton.2007.146

Hong, G., and Dai, H. (2016). In vivo fluorescence imaging in the second near-infrared window using carbon nanotubes. *Methods Mol. Biol. (Clifton, NJ).* 1444, 167–181. doi: 10.1007/978-1-4939-3721-9_15

Hong, G., Diao, S., Chang, J., Antaris, A. L., Chen, C., Zhang, B., et al. (2014a). Through-skull fluorescence imaging of the brain in a new near-infrared window. *Nat. Photonics* 8, 723–730. doi: 10.1038/nphoton.2014.166

Hong, G., Lee, J. C., Jha, A., Diao, S., Nakayama, K. H., Hou, L., et al. (2014b). Near-infrared II fluorescence for imaging hindlimb vessel regeneration with dynamic tissue perfusion measurement. *Circ. Cardiovasc. Imaging* 7, 517–525. doi: 10.1161/CIRCIMAGING.113.000305

International Commission on Non-Ionizing Radiation P (2013). ICNIRP guidelines on limits of exposure to laser radiation of wavelengths between 180 nm and 1,000 mum. *Health Phys.* 105, 271–295. doi: 10.1097/HP.0b013e3182983fd4

James, M. L., and Gambhir, S. S. (2012). A molecular imaging primer: modalities, imaging agents, and applications. *Physiol. Rev.* 92, 897–965. doi: 10.1152/physrev.00049.2010

Kim, T. H., and Schnitzer, M. J. (2022). Fluorescence imaging of large-scale neural ensemble dynamics. *Cells* 185, 9–41. doi: 10.1016/j.cell.2021.12.007

Kvetnansky, R., Sun, C. L., Lake, C. R., Thoa, N., Torda, T., and Kopin, I. J. (1978). Effect of handling and forced immobilization on rat plasma levels of epinephrine, norepinephrine, and dopamine-beta-hydroxylase. *Endocrinology* 103, 1868–1874. doi: 10.1210/endo-103-5-1868

Lauber, D. T., Fulop, A., Kovacs, T., Szigeti, K., Mathe, D., and Szijarto, A. (2017). State of the art in vivo imaging techniques for laboratory animals. *Lab. Anim.* 51, 465–478. doi: 10.1177/0023677217695852

Li, J., Ling, J., and Yao, C. (2022). Recent advances in NIR-II fluorescence based theranostic approaches for glioma. *Front. Chem.* 10:1054913. doi: 10.3389/fchem.2022.1054913

Li, B., Lu, L., Zhao, M., Lei, Z., and Zhang, F. (2018). An efficient 1064 nm NIR-II excitation fluorescent molecular dye for deep-tissue high-resolution dynamic bioimaging. *Angew. Chem. Int. Ed. Engl.* 57, 7483–7487. doi: 10.1002/anie.201801226

Li, H., Tan, M., Wang, X., Li, F., Zhang, Y., Zhao, L., et al. (2020). Temporal multiplexed in vivo upconversion imaging. *J. Am. Chem. Soc.* 142, 2023–2030. doi: 10.1021/jacs.9b11641

Linders, L. E., Supiot, L. F., Du, W., D'Angelo, R., Adan, R. A. H., Riga, D., et al. (2022). Studying synaptic connectivity and strength with optogenetics and patch-clamp electrophysiology. *Int. J. Mol. Sci.* 23:11612. doi: 10.3390/ijms231911612

Lundgaard, I., Li, B., Xie, L., Kang, H., Sanggaard, S., Haswell, J. D., et al. (2015). Direct neuronal glucose uptake heralds activity-dependent increases in cerebral metabolism. *Nat. Commun.* 6:6807. doi: 10.1038/ncomms7807

Mathis, A., Mamidanna, P., Cury, K. M., Abe, T., Murthy, V. N., Mathis, M. W., et al. (2018). DeepLabCut: markerless pose estimation of user-defined body parts with deep learning. *Nat. Neurosci.* 21, 1281–1289. doi: 10.1038/s41593-018-0209-y

Meijer, D. K., Weert, B., and Vermeer, G. A. (1988). Pharmacokinetics of biliary excretion in man. VI. Indocyanine green. *Eur. J. Clin. Pharmacol.* 35, 295–303. doi: 10.1007/BF00558268

Miranda, A., Glorie, D., Bertoglio, D., Vleugels, J., De Bruyne, G., Stroobants, S., et al. (2019a). Awake (18)F-FDG PET imaging of Memantine-induced brain activation and test-retest in freely running mice. *J. Nucl. Med.* 60, 844–850. doi: 10.2967/jnumed.118.218669

Miranda, A., Kang, M. S., Blinder, S., Bouhachi, R., Soucy, J. P., Aliaga-Aliaga, A., et al. (2019b). PET imaging of freely moving interacting rats. *NeuroImage* 191, 560–567. doi: 10.1016/j.neuroimage.2019.02.064

Noguchi, A., Ikegaya, Y., and Matsumoto, N. (2021). In vivo whole-cell patch-clamp methods: recent technical Progress and future perspectives. *Sensors (Basel, Switzerland)* 21:1448. doi: 10.3390/s21041448

Ortgies, D. H., Tan, M., Ximendes, E. C., Del Rosal, B., Hu, J., Xu, L., et al. (2018). Lifetime-encoded infrared-emitting nanoparticles for in vivo multiplexed imaging. *ACS Nano* 12, 4362–4368. doi: 10.1021/acsnano.7b09189

Ozbay, B. N., Futia, G. L., Ma, M., Bright, V. M., Gopinath, J. T., Hughes, E. G., et al. (2018). Three dimensional two-photon brain imaging in freely moving mice using a miniature fiber coupled microscope with active axial-scanning. *Sci. Rep.* 8:8108. doi: 10.1038/s41598-018-26326-3

Pare, W. P., and Glavin, G. B. (1986). Restraint stress in biomedical research: a review. *Neurosci. Biobehav. Rev.* 10, 339–370. doi: 10.1016/0149-7634(86)90017-5

Phinikaridou, A., Andia, M. E., Shah, A. M., and Botnar, R. M. (2012). Advances in molecular imaging of atherosclerosis and myocardial infarction: shedding new light on in vivo cardiovascular biology. *Am. J. Physiol. Heart Circ. Physiol.* 303, H1397–H1410. doi: 10.1152/ajpheart.00583.2012

Qian, Y., Piatkevich, K. D., Mc Larney, B., Abdelfattah, A. S., Mehta, S., Murdock, M. H., et al. (2019). A genetically encoded near-infrared fluorescent calcium ion indicator. *Nat. Methods* 16, 171–174. doi: 10.1038/s41592-018-0294-6

Ren, C., and Komiyama, T. (2021). Characterizing cortex-wide dynamics with wide-field calcium imaging. *J. Neurosci.* 41, 4160–4168. doi: 10.1523/JNEUROSCI.3003-20.2021

Sano, Y., Ito, S., Yoneda, M., Nagasawa, K., Matsuura, N., Yamada, Y., et al. (2016). Effects of various types of anesthesia on hemodynamics, cardiac function, and glucose and lipid metabolism in rats. *Am. J. Physiol. Heart Circ. Physiol.* 311, H1360–H1366. doi: 10.1152/ajpheart.00181.2016

Santos, H. D. A., Zabala Gutierrez, I., Shen, Y., Lifante, J., Ximendes, E., Laurenti, M., et al. (2020). Ultrafast photochemistry produces superbright short-wave infrared dots for low-dose in vivo imaging. *Nat. Commun.* 11:2933. doi: 10.1038/s41467-020-16333-2

Schoppe, O., Pan, C., Coronel, J., Mai, H., Rong, Z., Todorov, M. I., et al. (2020). Deep learning-enabled multi-organ segmentation in whole-body mouse scans. *Nat. Commun.* 11:5626. doi: 10.1038/s41467-020-19449-7

Schwarz, C., Plass, I., Fitschek, F., Punzengruber, A., Mittlbock, M., Kampf, S., et al. (2019). The value of indocyanine green clearance assessment to predict postoperative liver dysfunction in patients undergoing liver resection. *Sci. Rep.* 9:8421. doi: 10.1038/s41598-019-44815-x

Shemetov, A. A., Monakhov, M. V., Zhang, Q., Canton-Josh, J. E., Kumar, M., Chen, M., et al. (2021). A near-infrared genetically encoded calcium indicator for in vivo imaging. *Nat. Biotechnol.* 39, 368–377. doi: 10.1038/s41587-020-0710-1

Takuwa, H., Ikoma, Y., Yoshida, E., Tashima, H., Wakizaka, H., Shinaji, T., et al. (2016). Development of a simultaneous optical/PET imaging system for awake mice. *Phys. Med. Biol.* 61, 6430–6440. doi: 10.1088/0031-9155/61/17/6430

Tian, R., Ma, H., Zhu, S., Lau, J., Ma, R., Liu, Y., et al. (2020). Multiplexed NIR-II probes for lymph node-invaded cancer detection and imaging-guided surgery. *Adv. Mater.* 32:e1907365. doi: 10.1002/adma.201907365

Villette, V., Chavarha, M., Dimov, I. K., Bradley, J., Pradhan, L., Mathieu, B., et al. (2019). Ultrafast two-photon imaging of a high-gain voltage indicator in awake behaving mice. *Cells* 179, 1590–1608.e23. doi: 10.1016/j.cell.2019.11.004

Wang, W., He, X., Du, M., Xie, C., Zhou, W., Huang, W., et al. (2021). Organic fluorophores for 1064 nm excited NIR-II fluorescence imaging. *Front. Chem.* 9:769655. doi: 10.3389/fchem.2021.769655

Wang, Y., Xuan, J., Srikanchana, R., and Choyke, P. L. (2006). Modeling and reconstruction of mixed functional and molecular patterns. *Int. J. Biomed Imaging.* 2006, 1–9. doi: 10.1155/IJBI/2006/29707

Ximendes, E., Marin, R., Shen, Y., Ruiz, D., Gomez-Cerezo, D., Rodriguez-Sevilla, P., et al. (2021). Infrared-emitting multimodal nanostructures for controlled in vivo magnetic hyperthermia. *Adv. Mater.* 33:e2100077. doi: 10.1002/adma.202100077

Xu, J., Shi, R., Chen, G., Dong, S., Yang, P., Zhang, Z., et al. (2020). All-in-one theranostic nanomedicine with ultrabright second near-infrared emission for tumor-modulated bioimaging and chemodynamic/photodynamic therapy. *ACS Nano* 14, 9613–9625. doi: 10.1021/acsnano.0c00082

Yang, S., Tan, X., Tang, L., and Yang, Q. (2021). Near-infrared-II bioimaging for in vivo quantitative analysis. *Front. Chem.* 9:763495. doi: 10.3389/fchem.2021.763495

Yang, W., and Yuste, R. (2017). In vivo imaging of neural activity. *Nat. Methods* 14, 349–359. doi: 10.1038/nmeth.4230

Zhang, X. D., Wang, H., Antaris, A. L., Li, L., Diao, S., Ma, R., et al. (2016). Traumatic brain injury imaging in the second near-infrared window with a molecular fluorophore. *Adv. Mater.* 28, 6872–6879. doi: 10.1002/adma.201600706

Zhong, Y., Ma, Z., Wang, F., Wang, X., Yang, Y., Liu, Y., et al. (2019). In vivo molecular imaging for immunotherapy using ultra-bright near-infrared-IIb rare-earth nanoparticles. *Nat. Biotechnol.* 37, 1322–1331. doi: 10.1038/s41587-019-0262-4